Use of fly ash as synergistic and reactive component of flame retardant system in polylactide

Marcos Batistella, Jean Claude Roux, Gwenn Le Saout, Emanuela Callone, Sandra Dirè, Constantinos Xenopoulos, J. Lopez-Cuesta

Use of fly ash as synergistic and reactive component of flame retardant system in polylactide

Marcos Batistella [a,*], Jean-Claude Roux [a], Gwenn le Saout [b], Emanuela Callone [c], Sandra Diré [c], Constantinos Xenopoulos [d], José-Marie Lopez-Cuesta [a]

[a] Polymers Composites and Hybrids, IMT Mines Alès, Ales Cedex 30319, France
[b] LMGC, IMT Mines Ales, Université Montpellier, CNRS, Ales 30100, France
[c] "Klaus Müller" Magnetic Resonance Lab., Department of Industrial Engineering, University of Trento, Trento 38123, Italy
[d] Holcim Innovation Center, Saint Quentin Fallavier 38090, France

A B S T R A C T

For a long time, fly ash has been considered as pure waste of coal power plants. Nevertheless, unique properties and compositions that vary with the material's origin make fly ash appealing as an engineering material in various applications. Thus, the opportunity to reduce the environmental footprint of polylactide through the incorporation of fly ash as a component of flame retardant systems has been investigated. Combinations of fly ash with ammonium polyphosphate and/or melamine polyphosphate were made for a global loading of 25 wt% with various rates of substitution of the flame retardants. Fire performance has been studied from cone calorimeter experiments as well as the use of pyrolysis combustion flow calorimeter (PCFC) and the UL94V test. The interpretation of the fire retardant mechanisms has been performed through the examination of cone calorimeter residues by scanning electronic microscopy, X-ray microanalysis, X-ray diffraction (XRD) and multinuclear solid- state NMR. It can be shown that fly ash is mainly composed of spherical particles which are thermally stable at cone calorimeter tests when used alone in PLA. Conversely, fly ash behaves as a reactive component with both flame retardants, leading to the formation of new crystalline and amorphous compounds as shown by XRD and NMR. Synergistic effects in fire performance resulting from the reactive behavior of fly ash can be highlighted and are ascribed to fire retardant mechanisms acting in the condensed phase, and corresponding to the con-servation of high phosphorus contents in the condensed phase.

Keywords:
Polylactide
Fly ash
Fire behavior

1. Introduction

Nowadays, biobased polymers are able to replace fossil-based ones in many industrial applications. They were initially targeted to short-life applications, such as packaging in which longevity was not a high priority, but today more durable applications are envisioned requiring improvements in the resistance to various aging modes as well as to fire behavior. This results from the current requirements and standards in various sectors, such as building, transportation and electrical appliances. In the area of biopolyesters, since around 2005, various research studies have had as an objective to shift flame retardant systems and related knowledge from fossil–based polyesters to bio-based ones, mainly polylactide (PLA). Moreover, specific flame retardant systems or components devoted to biobased polymers were developed, in order to match the low environmental footprint of such polymers as well as to take into account their particular pathway of thermal degradation. According to different review articles, three main categories of flame retardant systems for PLA were identified: intumescent ones, mainly based on ammonium polyphosphate, new phosphorous and nitrogenous molecules, possibly issued from bio-based resources, and finally, natural or synthetic nanoparticles, possibly surface modified [1].

Intumescent systems are mainly composed of inorganic acids, acid salts or other acids able to dehydrate a carbonizing agent, which can be a carbohydrate or a polymer able to char, as well as a blowing agent such as melamine or urea [2,3].

Among possible acid sources, ammonium polyphosphate (APP) has been used predominantly in many research studies as well as in industrial compositions. APP has been also associated with lignin or starch [4–7] in partial or complete substitution with pentaerythritol which is the main carbohydrate used. Zhang et al. [8] have combined

* Corresponding author.
E-mail address: marcos.batistella@mines-ales.fr (M. Batistella).

Table 1
PLA formulations and nomenclature.

Formulation	PLA (wt%)	AP (wt%)	MP (wt%)	P (wt%)
PLA	100			
AP25	75	25		
P25	75			25
AP18.75P6.25	75	18.75		6.25
AP12.5P12.5	75	12.5		12.5
AP16.67MP8.33	75	16.67	8.33	
AP12.5MP6.25P6.25	75	12.5	6.25	6.25
AP8.33MP4.17P12.5	75	8.33	4.17	12.5

microencapsulated APP with lignin and organomodified montmorillonites (OMMT) whereas Carretier et al. [9] recently associated APP with lignin and sepiolite, another layered silicate. Other lamellar inorganic compounds were incorporated successfully in intumescent flame retardant systems for PLA such as layered double hydroxides (LDH) [10] or zirconium phosphate (ZrP) [11]. Zirconium phosphate (ZrP), layered double hydroxides (LDH), as well as halloysites were also organo-modified or synthesized in order to include phosphorous compounds [12–14] to be used alone or as hybrid flame retardants in PLA.

Various mechanisms were proposed by the authors to account for the contribution to the fire behavior of PLA of inorganic nanoparticles or ultrafine particles, possibly modified or combined with APP. Such particles are prone to exert barrier effects limiting the diffusion of heat and thermal gaseous degradation products as well as oxygen. This effect has been highlighted by Sonnier et al. through the combined use of combustion microcalorimetry (PCFC) and cone calorimeter [15]. It can be amplified by the ablation of the polymer exposed to the heat source as well as by the migration of the nanoparticles towards the exposed surface due to surface tension and viscosity effects resulting from temperature gradients [16]. A role of char promoter for the nanoparticles can also be highlighted through catalytic processes occurring at the surface of the nanoparticles during the degradation of PLA.

In the case of nanoparticles modified with phosphorous compounds, such as DOPO, Li et al. ascribed the improvement of fire retardancy to a progressive release of the phosphorous derivatives grafted on the surface of halloysites [14]. Another mechanism of fire retardancy was related to the reactivity of layered silicates towards phosphorous compounds and particularly APP. In the work of Carretier et al. [9], our research group highlighted the formation of silicon phosphate and other phosphorus compounds by reaction of sepiolite with APP, leading to synergistic effects on fire retardancy for APP/sepiolite mass ratio close to 6. Other kinds of silicates are able to react with APP to lead to new phosphorous species remaining in the condensed phase after thermal degradation. This is also the case of organomodified montmorillonites as shown by Vahabi et al. [17], Dumazert et al. [18]. These phenomena seems not to be restricted to layered silicates, since it has been noticed that chemical interactions occurred for water-based intumescent coatings based on ammonium polyphosphate containing fly ashes, boric acid, melamine and pentaerythritol [19].

Considering the world production of fly ashes (750 MT) and their potential use in engineering materials [20], the present article aims to assess the interest of the use of a specific fraction of fly ashes in flame retardant systems destinated for use with PLA and to highlight possible synergistic effects on fire properties. Cenospheres are mainly composed of amorphous glassy and various crystalline phases of aluminosilicates [21]. The opportunity to reduce the environmental footprint of a flame retarded PLA through the use of a mineral waste will be considered. Hence, substitutions of various types of components by fly ashes will be performed in flame retardant systems at constant global loading. The fire mechanisms related to these systems will be investigated through relevant techniques such as cone calorimeter and microcalorimeter in order to highlight possible interactions between the fly ashes and the other components, and particularly phosphorous/nitrogenous flame retardants.

2. Materials and methods

2.1. Materials

Polylactide (INGEO 4043D) was supplied by NatureWorks. Two flame retardants ammonium polyphosphate (Exolit™ AP422, from Clariant) noted AP and melamine polyphosphate (MP200, from BASF) noted MP were used. Fly ashes (SuperPozz) noted P with a median diameter of 6 μm and a specific surface area of 1.55 m^2/g were supplied by Holcim. Detailed composition obtained by X-fluorescence and X-diffraction Rietveld analysis are presented in supplementary information (Fig S1 and Table S1).

2.2. Methods

2.2.1. Processing

Various formulations containing binary and ternary blends at 25wt% were prepared using a twin-screw extruder (Clextral, France) with a feed rate of 5 kg/h and a temperature profile of 60–195 °C. The nomenclature used throughout is shown in Table 1.

2.2.2. Thermal analysis and fire testing

Thermal stability of composition was evaluated using a Setaram equipment (SETSYS Evolution) under nitrogen at 40 ml/min, from 30 to 750 °C with a temperature ramp of 10 °C/min.

The obtained pellets were injection molded using a Krauss Maffei equipment (KM 50t, temperature profile: 80–195 °C, mold temperature: 30 °C) to obtain square specimens of 100 × 100 × 4 mm^3 for cone calorimeter tests.

Cone calorimeter tests were carried out using an FTT equipment according to ISO 5660–1 with an irradiance of 50 kW/m^2. Three specimens (100 × 100 × 4 mm) were tested and mean values of Time to Ignition (TTI), peak of heat release rate (pHRR), total heat released (THR) and Maximum Average Rate of Heat Emission (MARHE) are given in the tables.

Underwriters Laboratory's UL-94 test (vertical burning test; ASTM D 380) which enables the assessment of the self-extinguishing time of materials was carried out on 90 × 10 × 4 mm samples. The classification is labelled as V0, the best, when the material is able to quickly extinguish the flame and presents a weak afterglow, without burning drips. V2 is the lowest ranking, when burning drips are observed, or when the material takes longer to extinguish the flame with burning drips.

Pyrolysis Combustion Flow Calorimeter (PCFC) (Fire Testing Technology) was initially developed by Lyon and Walters [22] to determine fire reaction parameters at microscale. Sample of around 3 mg were pyrolyzed in an inert gas at 1 °C/s to 750 °C. Then, the volatile thermal degradation products were sent to a furnace (combustor) with excess oxygen at 900 °C to force complete combustion. Heat release rate (HRR) was measured as a function of temperature, leading to the determination of the peak value of HRR as well as the Total Heat Release (THR) and Heat Release Capacity (HRC).

2.2.3. SEM and X-ray microanalysis

A Scanning Electron Microscopy (SEM) Quanta 200 FEG (FEI Company) operating in high vacuum at an acceleration voltage of 12.5 kV was used to observe the samples and the dispersion of fillers inside the polymer matrix as well as the combustion residues after cone calorimeter tests. For these observations, tensile test specimens were cryo-fractured and the central zone of the samples (perpendicular to the flow direction) were observed. Energy dispersive X-Ray spectroscopy was carried out on the combustion residues using an Oxford XmaxN system and a detector with a resolution of 133 eV.

2.2.4. X-ray diffraction

In order to evaluate a possible interaction between flame retardants and fly ash, X-ray diffraction of cone calorimeter residues were carried

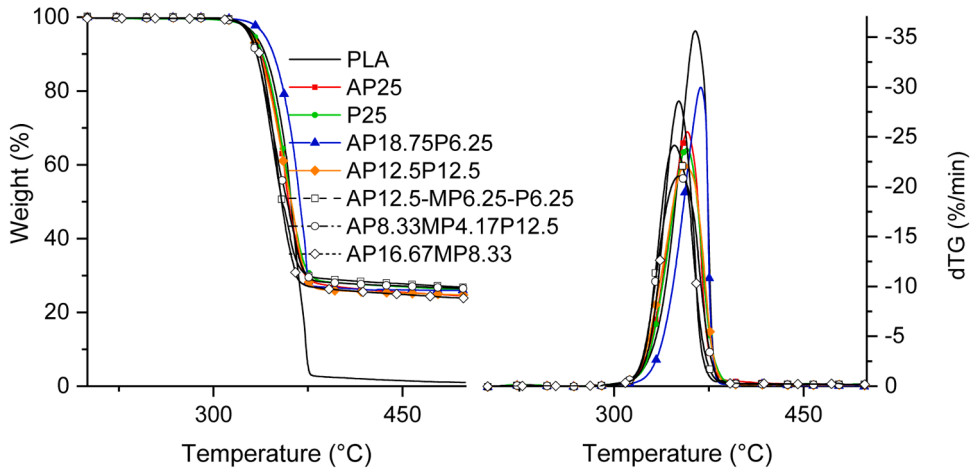

Fig. 1. Mass loss curves of PLA formulations, under nitrogen at 40 ml/min and 10 °C/min.

Table 2
Characteristic degradation temperatures of PLA formulations under nitrogen at 10 °C/min.

Formulation	$T_{5\%}$ (°C)	$T_{20\%}$ (°C)	$T_{50\%}$ (°C)	Residue at 750 °C (%)
PLA	333	349	362	–
AP25	331	346	360	21
P25	332	347	362	23
AP18.75P6.25	341	355	369	26
AP12.5P12.5	330	345	362	22
AP16.67MP8.33	331	342	354	20
AP12.5MP6.25P6.25	330	340	354	22
AP8.33MP4.17P12.5	329	341	358	23

out on an D8 Advance diffractometer (Bruker AXS with CuKα radiation and a Lynxeye detector) in the 5–70° 2θ range with a steep size of 0.007°

2.2.5. Solid state nuclear magnetic resonance

All the solid state NMR analyses were performed on residues with a 9.4 T Bruker Avance 400WB spectrometer equipped with a double resonance CPMAS probe under Magic Angle Spinning (MAS) using single pulse sequence. Typical experimental parameters are: ^{31}P) frequency of 161.97 MHz, π/4 flip angle of 3.9 μs, recycle delay of 120 s and 128 transients; ^{27}Al) frequency of 104.26 MHz, π/12 flip angle of 2 μs, recycle delay of 1 s and 1k transients; ^{29}Si) frequency of 79.57 MHz, π/4 flip angle of 2.2 μs, recycle delay of 100 s and 2k transients. Samples were packed in 4 mm zirconia rotors, which were spun at 12 kHz under air flow.

Octakis(trimethylsiloxy)silsesquioxane (Q_8M_8), $Al(NO_3)_3$ 1 M and diphosphatidic acid (ADP) were used as external secondary references. Usual notation for silicates and phosphates in ^{29}Si and ^{31}P NMR are used: Q^n stands for $Si(OSi)_n(OX)^{4-n}$ (X = H or either heteronucleus such as Al), Q'^n stands for $OP(OP)_n(OX)^{3-n}$ (X = *H* or either heteronucleus such as Si). Profile fitting analyses were performed assuming Gaussian/Lorenzian lineshapes for half integer spin nuclei and Czjzek model [23] for quadrupolars with Topspin 3.6 and DMfit [24] softwares, with a confidence level of 95%.

3. Results and discussion

3.1. Scanning electronic microscopy of initial samples

From the SEM pictures, (Figure S2), it can be noticed that all the components are well dispersed in the polymer. Fly ash spheres are clearly identified and exhibit a large particle size distribution (Figure S2-F). AP particles present the highest particle size and show a faceted surface (Figure S2-D).

3.2. TGA results

Mass loss and derivative mass loss curves of all compositions are presented on Fig. 1 and some characteristic degradation temperatures

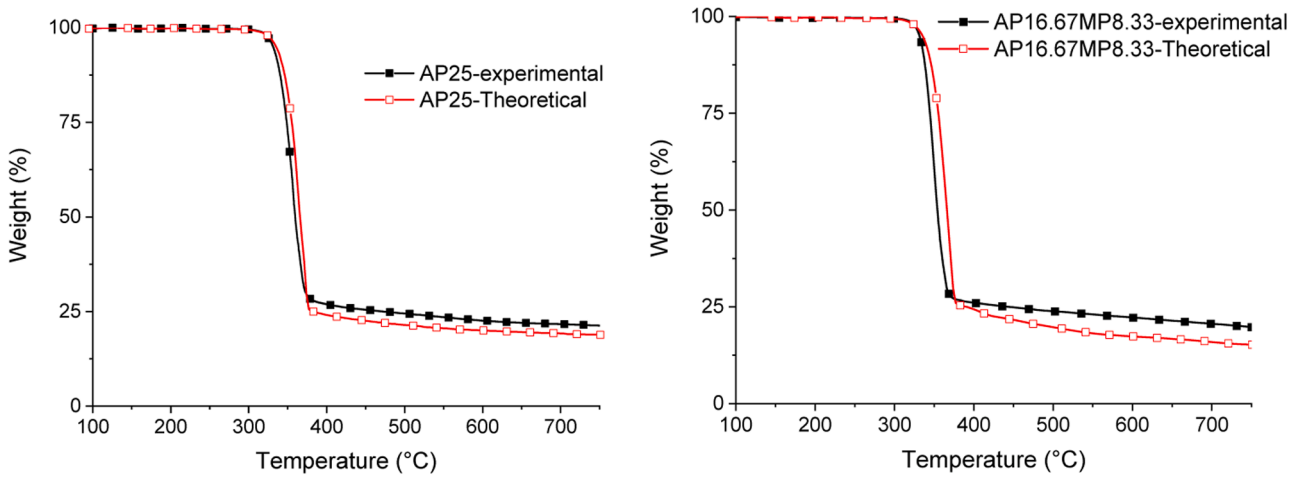

Fig. 2. Comparison of experimental and theoretical mass loss curves of AP25 and AP16.67MP8.33 formulations.

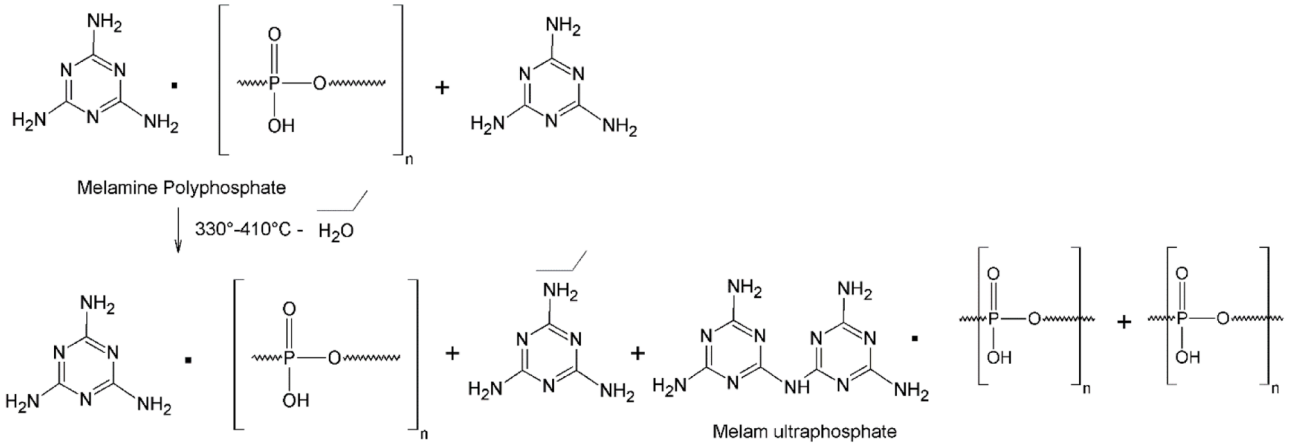

Fig. 3. Thermal decomposition of melamine polyphosphate (from Costa et al. [27]).

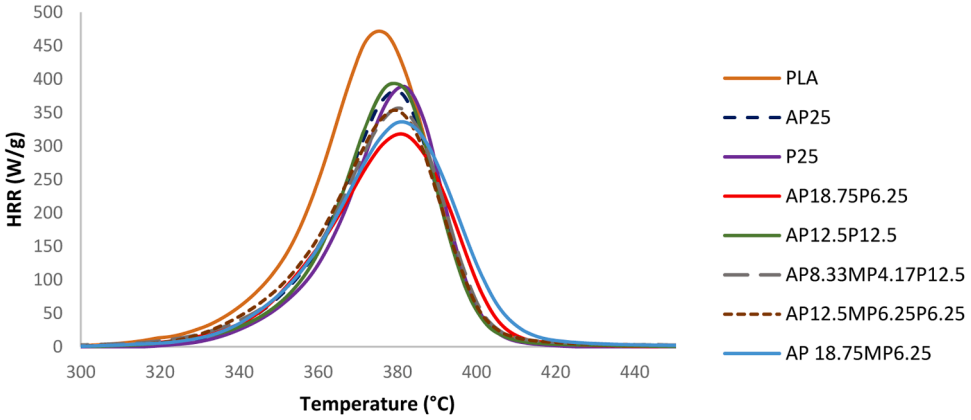

Fig. 4. PCFC curves of HRR as function of time for all PLA compositions.

Table 3
PCFC results for all PLA compositions.

Sample	HRC (J/g/K)	pHRR (W/g)	THR (J/g)	TpHRR (°C)
PLA	480	473.2	17.4	375.8
AP25	386	388.2	12.2	379.8
P25	402	393.8	12.4	379.4
AP18.75P6.25	325	318.0	12.7	381.2
AP12.5P12.5	412	396.2	12.4	379.4
AP16.67MP8.33	346	339.0	13.4	381.5
AP8.33MP4.17P12.5	361	356.2	12.6	380.9
AP12.5MP6.25P6.25	358	349.6	12.8	377.5

corresponding to the temperature of 5wt%, 20wt% and 50wt% mass loss ($T_{5\%}$, $T_{20\%}$ and $T_{50\%}$ respectively) are presented on Table 2. PLA decomposes in one step without formation of a stable residue. It appears that all the flame retarded compositions exhibit very similar thermograms. Comparing PLA and PLA compositions mass loss curves, it can be noticed that they are superimposed, indicating that fly ash and flame retardants alone or in binary/ternary compositions do not seem to modify the thermal stability of PLA. This conclusion is further supported by characteristic degradation temperatures, which are very close to neat PLA. Interestingly, only the composition with 18.75wt% AP and 6.25wt % P entails an increase of thermal stability of PLA (increase on $T_{5\%}$, $T_{20\%}$ and $T_{50\%}$) as well as a bigger amount of residue which could result from the formation of new chemical structures in the condensed phase as well as a charring of the sample. The observed behavior can be explained by the thermal degradation of components. AP decomposes firstly into phosphoric acid and ammonia [2]. The formation of char from PLA is catalyzed by the presence of the phosphoric acid, which also reacts with the ester end groups of the polymer, leading to carbon dioxide [25]. If decompositions of AP and PLA are considered separately (Fig. 2), it can be highlighted that the interaction of both those two components is limited. Indeed, experimental (AP 25) and theoretical curves are very close and the final residue amounts are similar. Consequently, it can be deduced that the phosphorylation of PLA by APP is limited. MP combines the advantages of phosphorus and melamine-based flame retardants. It is able to promote both charring and formation of strongly crosslinked phosphorous and carbonaceous structures [26]. Moreover, according to Costa et al. [27], melamine is released from MP around 400 °C (Fig. 3). This allows to promote the expansion of the formed structures but also to entail an endothermal effect due to the decomposition of melamine. The interest in MP as a flame retardant of PLA was highlighted by Guo et al. [28] who investigated MP and organomodified montmorillonite compositions processed using additive manufacturing. Similarly to the AP25 composition, a theoretical thermogram corresponding to AP16.67MP8.33 composition was compared to the experimental one.

3.3. *Pyrolysis combustion flow calorimetry*

HRR curves of PCFC tests are presented on Fig. 4 and complete results (Heat Release Capacity (HRC), peak of Heat Release Rate (pHRR), Total Heat Released (THR) and temperature of pHRR (TpHRR)) on Table 3. All the compositions allow a significant reduction of HRC, pHRR and THR values and very similar values of total heat released of PLA compositions are noted. For all compositions, the temperature of

Table 4
Cone calorimeter results of compositions.

Formulation	TTI (s)	pHRR (kW/m^2)	THR (MJ/m^2)	MARHE (kW/m^2)	Residue (wt%)	UL94
PLA	62 ± 3	496 ± 45	90 ± 2	281 ± 30	0	NC
AP25	65 ± 2	286 ± 38	80 ± 2	187 ± 28	19 ± 1	V-0
P25	50 ± 1	332 ± 25	82 ± 1	265 ± 42	25 ± 1	V-2
AP18.75P6.25	58 ± 2	269 ± 29	72 ± 2	124 ± 35	32 ± 2	V-2
AP12.5P12.5	53 ± 2	336 ± 32	82 ± 1	185 ± 24	22 ± 2	V-2
AP16.67MP8.33	56 ± 1	199 ± 20	83 ± 2	87 ± 22	44 ± 2	V-0
AP12.5MP6.25P6.25	51 ± 3	194 ± 15	80 ± 1	84 ± 28	42 ± 1	V-0
AP8.33MP4.17P12.5	53 ± 2	294 ± 12	81 ± 1	156 ± 15	21 ± 2	V-2

pHRR is slightly increased, which indicates a fire retardant effect of the additives. Comparison of pHRR values for AP25, P25, AP18.75P6.25 and AP12.5P12.5 enables to highlight a synergistic effect between the two components for a minor percentage of fly ash. The association with both flame retardants also leads to a synergistic effect, indicating chemical interactions among the components as proved by the new compounds/structures detected through XRD and NMR (see Sections 3.6 and 3.7). Compositions of fly ash with AP and MP seems less interesting than AP18.75P6.25 composition, nevertheless these compositions appear more interesting than the only use of AP.

3.4. Cone calorimeter and UL94 results

Results of fire tests are presented in Table 4 and Fig. 5. AP used alone leads to a noticeable improvement of fire retardancy in comparison with pristine PLA. The percentage of residue obtained is close to the one obtained from TGA measurements. The association of AP and MP leads to a synergistic effect on fire properties and to a considerable increase of the residue up to 44% of the initial weight. Previously Fontaine and Bourbigot had shown the interest in combining ammonium polyphosphate and melamine in PLA [29]. An optimal percentage of AP/melamine ratio was found on the basis of cone calorimeter tests at 35 kW/m^2. This can be ascribed to the role as a foaming agent of melamine but also to an enhanced formation of ultraphosphate promoted by an optimal melamine/AP combination in comparison to AP alone.

Fly ash used alone acts positively on the fire reaction by reducing pHRR. TTI is slightly reduced, possibly due to an increase of thermal conductivity, leading to a wick effect. Despite the fact that inorganic components of the fly ash are not able to form glassy structures, it can be assumed that their submicronic fraction can migrate towards the exposed surface to the radiant flux due to temperature gradients affecting viscosity and surface tension of the polymer, leading to the formation of a mineral protective layer during thermal degradation of the polymer. This phenomenon has been highlighted for several types of nanoparticles, in particular for organomodified layered silicates [30]. Ultrafine fly ashes may also increase the viscosity of polymer, thereby limiting the ability for degraded products to feed the gaseous phase. Nevertheless, the self-extinguishability of this composition is limited since only a V-2 ranking is recorded.

Two compositions associate AP and P, while maintaining the global loading constant at 25wt%. An equimassic composition of the two components leads to pHRR values that are relatively close to those of AP alone, but the HRR profile is completely different. The reduction of AP leads to a reduced action of the mechanism of char promotion in the first stages of combustion, particularly for AP12.5P12.5 composition. However, the presence of fly ashes allows a stronger decrease of HRR after the peak to a lower level in comparison with APP only (around 100 kW/m^2) despite HRR increasing again afterwards.

An AP/P weight ratio of 2:1 can be shown to lead to a synergistic effect on all the cone calorimeter parameters to be highlighted. The HRR profile is similar to that of the other mixed composition, but HRR values lower than 50 kW/m^2 can be obtained just after 150 s. pHRR, HRR, MAHRE are significantly reduced in comparison with AP alone. It appears clearly that the combustion duration is increased, suggesting a lower mass loss kinetics. Moreover, a dramatic increase of the amount of the residue is noticed in comparison with AP and P composition considered separately. This suggests further that new reactive processes between the polymer and the two components have occurred to form cohesive protective layers at the surface of the residual polymer. However, this combination does not reach V-0, the level of self extinguishability attained by AP alone.

Since a synergistic effect has been observed between AP and MP, two ternary compositions were further examined, keeping the ratio between the two FRs constant at 2:1, but with a substitution of 25% and 50% of the global loading. In the first case, it can be noticed that the presence of P allows the fire performance to be maintained. The HRR profile is entirely similar to the AP/MP composition with also very similar fire parameters with a comparable amount of residue. In addition, the V-0 ranking is maintained. Consequently, it shows that the presence of fly ash is able to build cohesive protective layers exhibiting a similar level of cohesion and performance to the ultraphosphates generated by the AP/MP combination. Nevertheless, the formation of

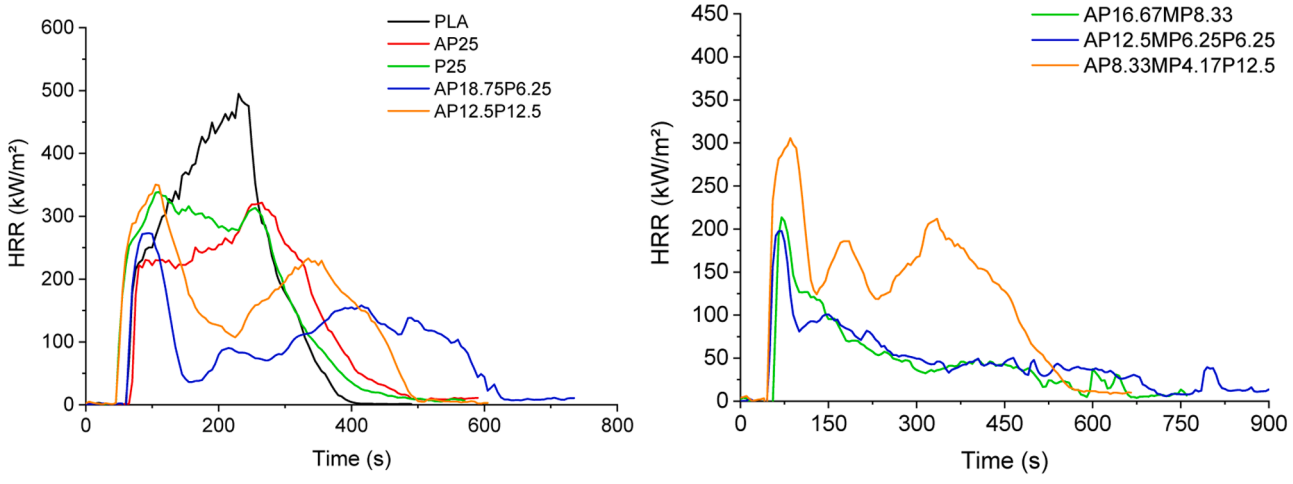

Fig. 5. Heat Release Rate curves of compositions (Irradiance 50 k/m^2).

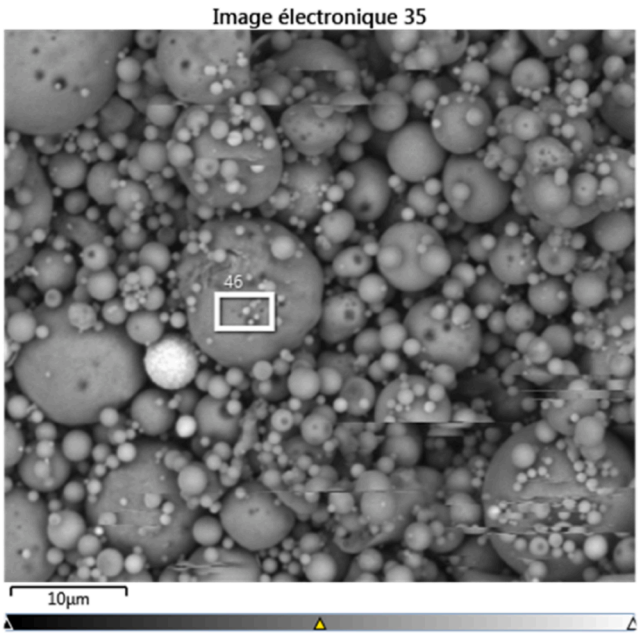

Fig. 6. SEM micrograph of cone calorimeter residue for P25 composition corresponding to X-ray microanalysis characterization.

Table 5
Composition of cone calorimeter residues.

Formulation	Al (wt %)	Si (wt %)	Fe (wt %)	C (wt %)	P (wt %)	N (wt %)	Phosphorus balance (%)
AP25	0.3	–	–	35	22	4	28
P25	20	24	3	–	–	–	–
AP18.75P6.25	4	5	0.5	18	24	–	73
AP12.5P12.5	6	7	1	9	22	–	69
AP16.67MP8.33	–	–	–	27	23	6	85
AP12.5MP6.25P6.25	3	4	0.6	28	19	–	93
AP8.33MP4.17P12.5	6	8	0.6	20	16	–	59

such structures is governed by stoichiometric relations between the components since a 50wt% substitution does not lead to the same level of performance. It is also noted to consider that based on the cone calorimeter data, the AP8.33MP4.17P12.5 composition behaves very similarly to AP25, from the cone calorimeter data, with even a better value of MARHE. Nevertheless, only V-2 is obtained with this composition.

The addition of flame retardants and fly ash leads to a decrease on THR compared to neat PLA, with a higher decrease for the AP18.75P6.25 formulation. Furthermore, MARHE values decrease compared to neat PLA, with better performances for AP16.67MP8.33 and AP12.5MP6.25P6.25 formulations which can be attributed to the formation of a protective surface layer, with very low HRR values following the pHRR.

Lewin and Weil [31] tried to quantify the synergistic effects of additives used in flame retardant compositions using a synergistic effectiveness (Es) parameter. Based on a given flammability parameter (Fp) the synergistic effectiveness can be calculated as follows:

$$E_s = \frac{\{(F_{p[fr+s]} - F_{p[p]})\}}{\{(F_{p[fr+s]} - F_{p[p]}) + (F_{p[s]} - F_{p[p]})\}}$$

Where $(F_P)_p$ is the flame retardant property of the neat polymer, $(F_P)_{fr}$ is the same property of the polymer containing the flame retardant, $(F_P)_s$ corresponds to the polymer containing the additive or synergist and $(F_P)_{fr+s}$ is the full formulation containing both the FR and the synergist. The proposed parameter allows the comparation of synergistic properties to be made: if Es > 1, some synergistic effects may occur. For additive systems Es $= 1$ and for less than additive systems Es < 1. Results of the effectiveness parameter based on pHRR, HRC and MARHE are given on Table S2. It can be seen that, depending on the amount of fly ash, a less than additive system is observed for pHRR and HRC parameters. Moreover, comparing MARHE values, a synergistic effectiveness can be observed for the AP18.75P6.25 formulation, that could be related to formation of new species when the ration between FR and fly ash is 2:1.

3.5. SEM observations and X-ray microanalysis of cone calorimeter residues

The observation of P25 residue is very similar to the pristine fly ash alone. Fig. 6 displays a very broad particle size distribution of spheres, from submicronic scale to around 20 µm. X-ray microanalyses performed on a large population of particles as well as individual big particles indicate the presence of mainly Si (24wt%), Al (20wt%), and Fe (3wt%) (Table' 5). There is no carbonaceous residue. Consequently, the leveling off of the HRR values for P25 in comparison with that of a pure

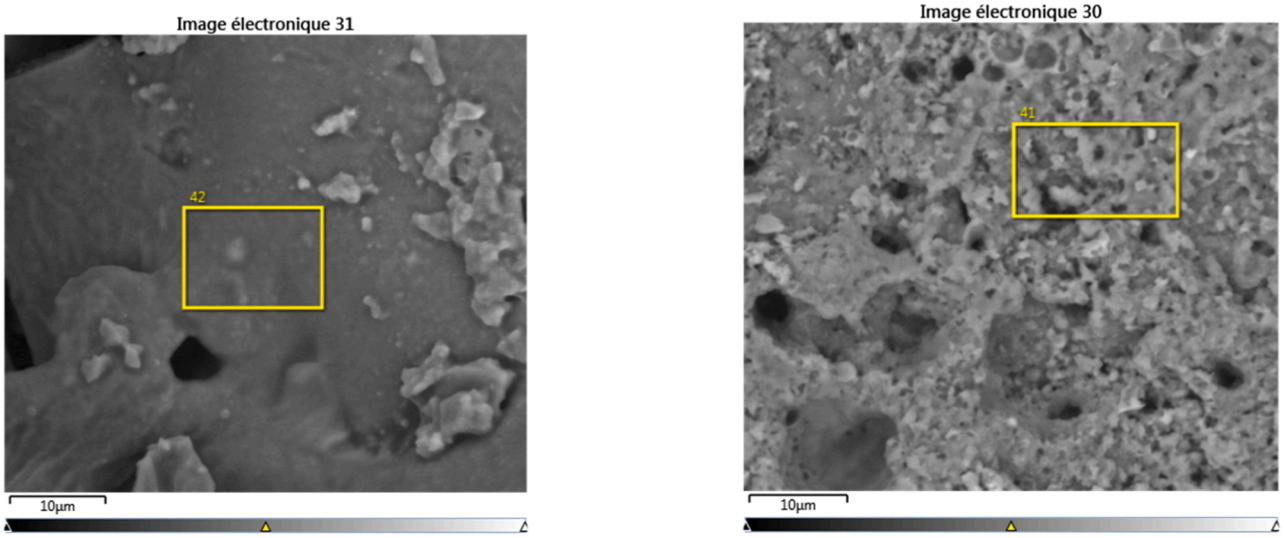

Fig. 7. SEM micrograph of cone calorimeter residue for AP25 composition corresponding to X-ray microanalysis characterization (external surface (left), internal surface (right)).

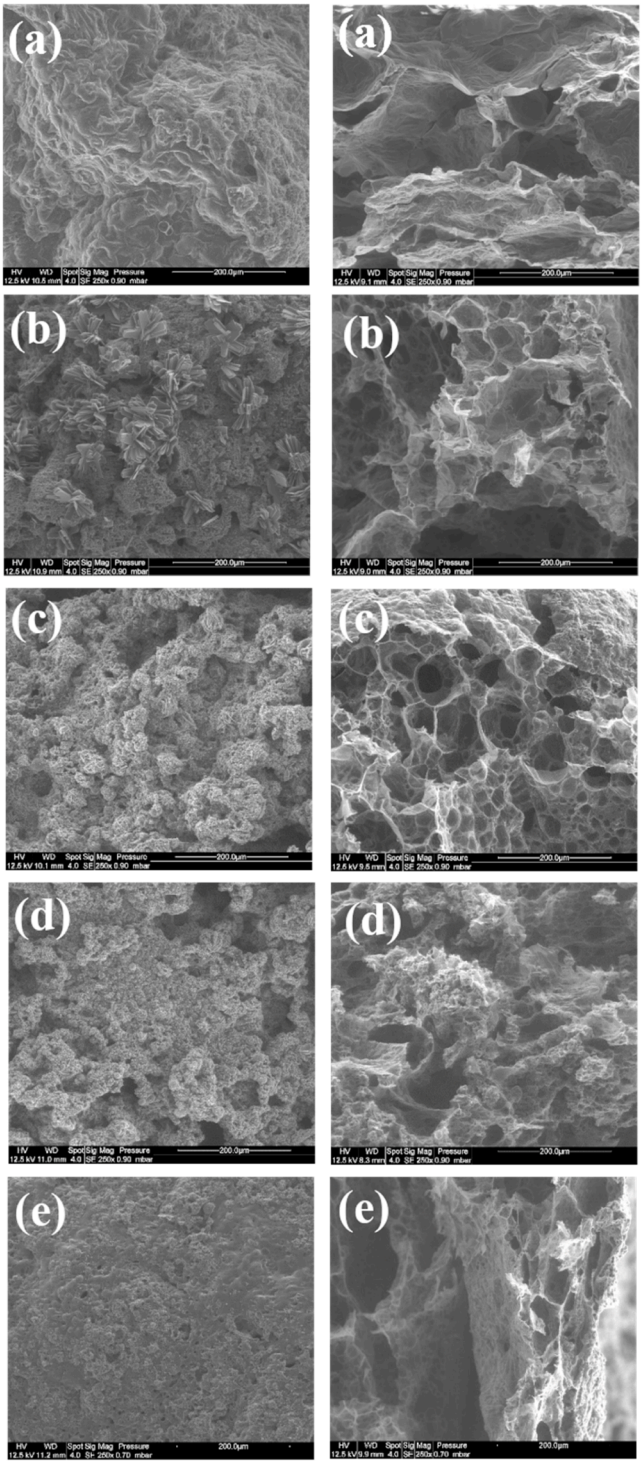

Fig. 8. SEM micrographs of cone calorimeter residue for a) AP16.67MP8.33 b) AP18.75P6.25 c) AP12.5P12.5 d) AP8.33MP4.17P12.5 e) AP12.5MP6.25P6.25 compositions, (external surface (left), cross section (right)).

PLA curve could be ascribed to the ablation of a fraction of polymer exposed to the heat flux leading to a surface mainly composed of spherical ash particles able to create a barrier effect for the diffusion of volatiles and oxygen due to the compact packing of its particles.

As shown to X-ray microanalysis micrograph in Fig. 7, AP25 residue presents a cohesive external surface whereas the internal section of the residue reveals a microporous structure. High amounts of carbon and phosphorus are detected (Table 5). AP16.67MP8.33 behaves similarly (Fig. 8a) with a cohesive external surface and a microporous cross section. Conversely, compositions containing both AP and P presents a completely different external structure with the formation of crystallized platelets organized similarly to windroses (Fig. 8b and c). For all these compositions, the cross section appears microporous. The two combinations of both FRs with fly ash exhibit dissimilar aspects for the external surface, whereas this of AP8.33MP4.17P12.5 appears close to that of AP12.5MP6.25P6.25, with pores and nodular structures made of crystallized platelets (Fig. 8d), AP12.5MP6.25P6.25 residue appears more compact and platelets appear only at a very small scale on the SEM picture, at the micronic or submicronic level (Fig. 8e). However, the cross section looks like to all previous compositions with macropores. An observation of the external surface of all residues at higher magnification shows the presence of residual ash particles, particularly for AP18.75P6.25 (Fig. 9).

3.6. X-ray microanalysis of cone calorimeter residues

Semi-quantitative analyses of compositions were carried out to investigate the global composition of residues as well as specific areas corresponding to selected particles. Table 5 reports the elementary percentages of mainly carbon, phosphorus, silicon and aluminum. The phosphorus balance corresponds to the quantity of phosphorus remaining in the residue relative to the initial amount in the sample.

A comparison of the values for AP25 and AP18.75P6.25 indicates a similar level in phosphorus percentage for the mixed composition. Taking into account the higher percentage of residue, even after subtracting the remaining percentage of fly ash, it appears that the amount of phosphorus retained in the residue is higher for the mixed composition (higher P balance). However, this effect seems less significant for the AP12.5P12.5 composition as well as for the AP8.33MP4.17P12.5 composition. Conversely, AP12.5MP6.25P6.25, the ternary composition with the lower fly ash amount exhibits a rather high phosphorus percentage as well as a very high amount of residue and, as it turns out, finally the highest P balance. As for AP18.75P6.25, it can be suggested that new compounds combining phosphorus and components of fly ash have been formed during the thermal degradation. Hence, it appears that for these last compositions fire retardant mechanisms occurring in the condensed phase are predominant. Moreover, the conservation of the main fraction of phosphorus in the residue seems to lead to the higher level of fire performance.

3.7. X-ray diffraction of cone calorimeter residues

XRD has been performed on ground and homogenized cone calorimeter residues as well as neat fly ash (Fig. 10). XRD patterns of the residues show the presence of the initial fly ash (crystalline phases mullite, quartz and the hump assigned to the amorphous part. Various new crystalline structures appear for AP18.75P6.25 which could correspond to the crystallized platelets but remains difficult to identify. In the previous work of Puri et al. [19], the formation SiP_2O_7, $AlPO_4$ and $Al(PO_3)_3$ were pointed out but not found here. Conversely, the peaks observed for AP12.5MP6.25P6.25 allow new ammonium aluminum phosphate ($NH_4AlP_2O_7$) and hydrogenophosphate ($Al(NH_4)HP_3O_{10}$) to be identified. This could highlight the important role of MP in order to form a cohesive structure at the surface of the residue. These compounds might be able to reinforce the char formed containing ultraphosphate species resulting from the interactions between PLA, AP and MP during the thermal degradation.

3.8. NMR on cone calorimeter residues

The XRD study of fly ash and the selected AP18.75P6.25 and AP12.5MP6.25P6.25 compositions were complemented with a multinuclear solid state NMR analysis in order to obtain an overall picture of the composition of the burned products.

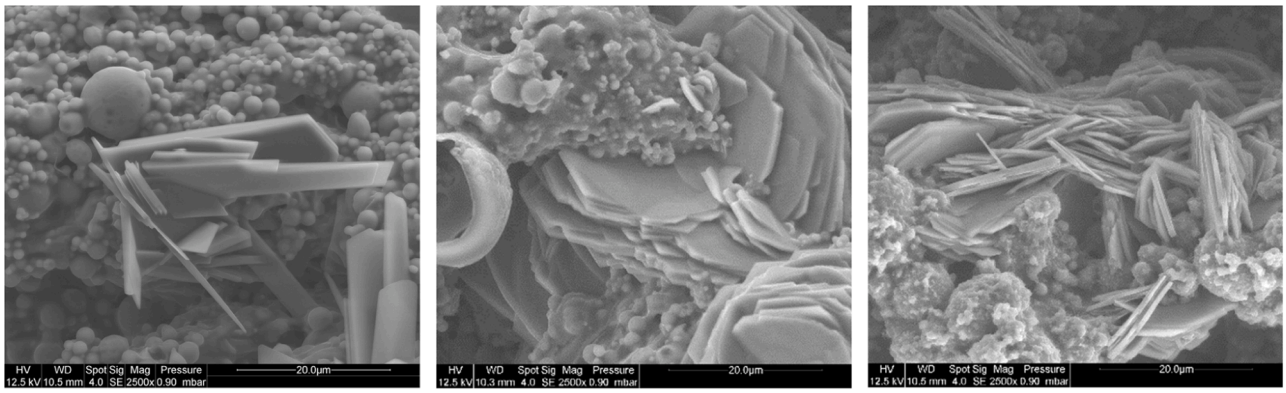

Fig. 9. SEM micrographs of cone calorimeter residue for AP18.75P6.25 (left)) AP12.5P12.5 (middle) AP8.33MP4.17P12.5 (right) composition showing platelet-like crystallized structures.

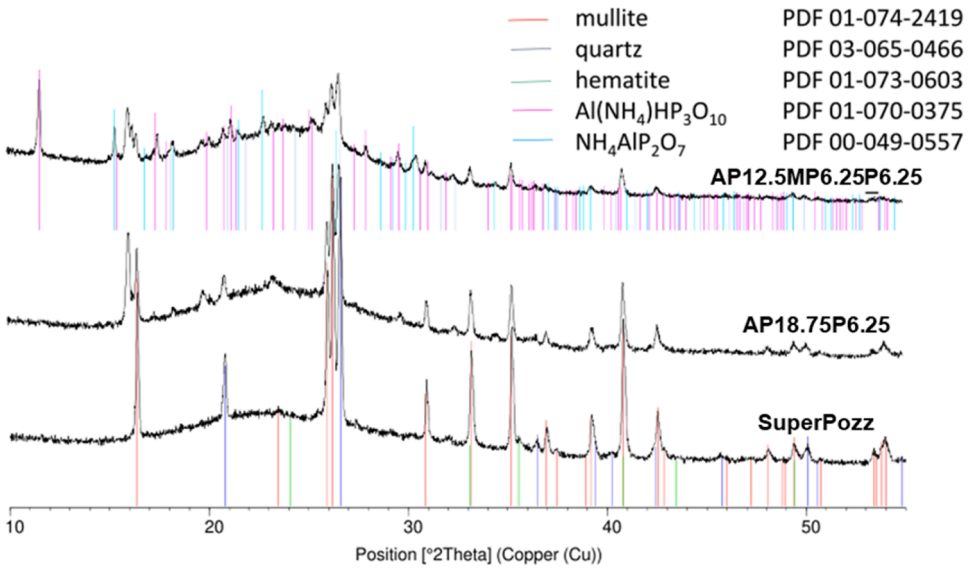

Fig. 10. XRD results of selected cone calorimeter residues.

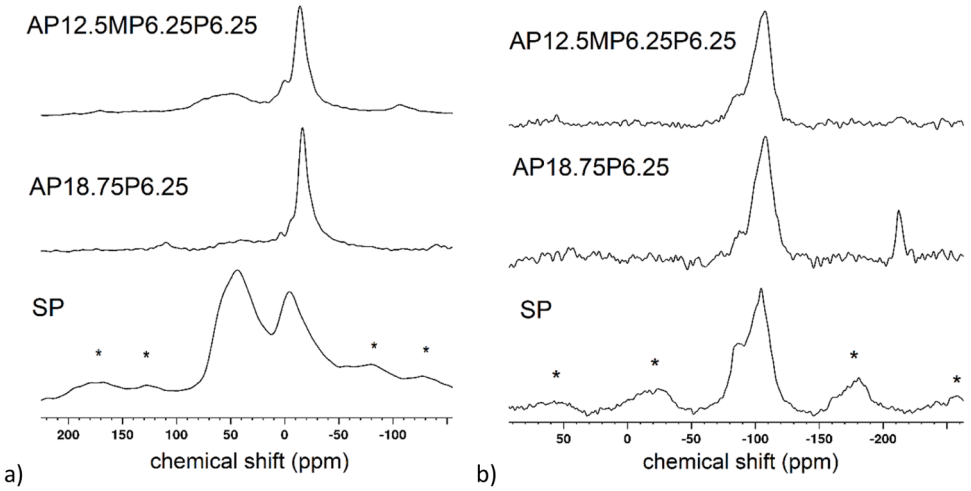

Fig. 11. (a) ^{27}Al MAS NMR spectra and (b) ^{29}Si MAS NMR spectra of fly ash and AP18.75P6.25 and AP12.5MP6.25P6.25 samples. The ssb are marked with*.

Due to the aluminosilicate nature of fly ash, the ^{27}Al and ^{29}Si MAS spectra of SP were compared with the two selected residue samples in Fig. 11a and b. The broadness and the wide spinning sideband (ssb) - manifold characterizing the resonances are due to the presence of iron oxide. This also suggests the need for caution in regard to the quantitative analysis of fly ash due to possible partial signal loss [32].

Table 6
Quantitative analysis of ^{27}Al spectra with peak assignment.

δ(ppm)	68.4	46.6	28.5	7.1	−2.1	−13.3
Assign.	T_d	T_d	Al^V	O_h	O_h	O_h
	%					
P	23.8*	35.2*	5.4		35.6*	
AP18.75P6.25	2.3	15.8		2.8	1.5	77.7
AP12.5MP6.25P6.25	10.7	20.3		1.6	2.4	65.0

* as indicated in the text the SP resonances are centered at slightly different chemical shifts (70.8, 51.4 and −3.6 ppm, respectively) with respect to the reported values for residue samples.

The ^{27}Al MAS spectrum of the fly ash is characterized by the presence of two overlapped resonances centered at about +71 and +51 ppm (attributed to Al-O-Al and Al-O-Si in tetrahedral sites (T_d), respectively and accounting for 59%), and one resonance due to Al-O-Al in octahedral units (O_h) centered at −3.6 ppm, accounting for 36%. Moreover, another resonance due to Al^V at +28.5 ppm (5%) could also be taken into consideration (an example of profile fitting is proposed in supplementary materials Figure S3) [33–36]. On the contrary, the spectra of the residues AP18.75P6.25 and AP12.5MP6.25P6.25 show a much sharper dominant O_h resonance with two small left shoulders and the T_d contribution appears significantly reduced. This is especially true for AP18.75P6.25 sample. An attempt of quantitative analysis is reported in Table 6.

The assignment of the three O_h components in the composites is not trivial. However, on the basis of what has previously been reported in the literature, some attempts could be made. The main resonance (−13.3 ppm) can be attributed to octahedral Al bonding three or less phosphate ions [37]. The O_h shoulder at 7 ppm presents similar position of amorphous nano-aluminate hydrate surface phases or hydrotalcite-like phases, whose resonance slightly shifts according to the intercalated anions [38]. The other small shoulder at −2 ppm could be ascribed to Al^V in AlPO structures that are not detected with XRD in the present case [39]. Thus, the signals can be attributed to both the identified crystalline phases and the glassy or amorphous Al-O-P compounds [40].

The ^{29}Si spectrum of fly ash is characterized by a broad resonance at around −100 ppm, as a result of the overlapping of different components, such as silica at −111 and −101 ppm (Q^4, Q^3, i.e. silicon atoms

Table 7
Quantitative analysis of ^{29}Si spectra with peak assignment.

δ(ppm)	−88.8	−101.3	−105.7	−107.7	−111.0	−215.9
Assign.	$Q^3(1Al)$	Q^3	*quartz*	$Q^4(1Al)$	Q^4	Si^{VI}
	%					
P	34.4		1.1	64.4		
AP18.75P6.25	7.8	7.6	3.0		71.2	10.4
AP12.5MP6.25P6.25	13.9	23.6	1.3		58.5	2.7

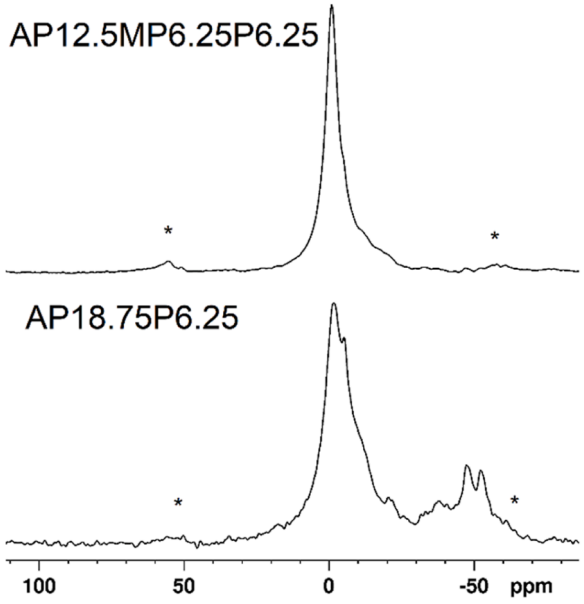

Fig. 12. ^{31}P MAS NMR spectra of AP18.75P6.25 and AP12.5MP6.25P6.25 samples. Ssb are marked with*.

Table 8
Quantitative analysis of phosphorus-31 spectra with peak assignment.

δ(ppm)	−1,1	−6,0	−11,2	−19,8	−37,6	−47,7	−52,8
Assign.	*Q'$_2$, metal phosphon., end phosph. groups, P-O-C, Pyrophosph.*			*Original/cyclic. polyphosph.*	*Q'$_3$ linear polyphosph.*	*O = P(OP/Si)$_3$*	*O = P(OP/Si^{VI})$_3$*
	%						
AP18.75P6.25	42,5	9,1	18,5	5,1	10,7	8,3	5,8
AP12.5MP6.25P6.25	83,1	8,8	3,1	4,9	< 1	< 1	< 1

connected through bridging oxygens to 4 and 3 Si, respectively), quartz at − 105 ppm, and components at − 107 and − 89 ppm due to mullite, in agreement with aluminum-27 and XRD findings [33], with replacement of Si by Al in a tetrahedral environment (Q^4(1Al), Q^3(1Al), i.e. silicon atoms connected through bridging oxygens to 3 and 2 Si and 1 Al^{IV}, respectively). Again, in both residues the fly ash structure is modified: the aluminum-substituted units significantly decrease in favor of pure silica units (Q^3, Q^4), suggesting a phase separation. Moreover, a certain amount of 6-fold coordinated Si is present in AP18.75P6.25 sample and also, but in almost negligible fraction, in AP12.5MP6.25P6.25 sample. It is represented by the resonance centered at − 216 ppm, and could be assigned to structures such as $Si_5O(PO_4)_6$. [41–43]. The quantitative analysis with assignment is reported in Table 7.

A clear interaction between the intumescent P-based compounds and the fly ash has been demonstrated by the highlighted structural changes imparted on fly ash, especially in the binary composition with AP alone. Accordingly, ^{31}P NMR analyses can complete the picture, evaluating the modifications at the expenses of both AP and MP, which both show up in the phosphorus-31 spectrum a doublet in the range from − 19 to − 23 ppm, according to the literature [44,45].

In both composite spectra (Fig. 12 and Table 8), the very low intensity of the resonance at about − 20 ppm indicates the almost complete decomposition of the long chain polyphosphate structure of the P-based compounds. Moreover, the sharpness of the resonances in Fig. 12 suggests that the thermal treatment induces the formation of slightly ordered phosphate structures. The main contribution around 0 ppm originates from the overlapping of three components centered at − 1, −6, −11 ppm, whereas the former is more pronounced in AP18.75P6.25. The resonances in this region are usually attributed to P-O-C groups, or end-chain phosphate groups or metal phosphonates and pyrophosphates [46]. In fact, they could be the result of the thermal reaction between the phosphate groups and the great amount of organic C of PLA, the released Al from fly ash and the other cations characterizing the fly ash such as Ca^{2+} or Mg^{2+}. Moreover, the possible presence of end-chain phosphate groups is consistent with a reduced phosphate chain length. Furthermore, according to XRD results and the quantitative analysis they could reasonably also be assigned to new ammonium aluminum phosphate and hydrogenophosphate phases.

The other resonances, detected mainly in the binary AP18.75P6.25 could be assigned as follows. The broad peak at around – 30 ppm is assigned to Q'_3 species in polyphosphates. The high-field components should be associated to amorphous phosphosilicates (at about −47 ppm and −53 ppm) such as structures with [PO_4] unit linked to both Si^{VI} and Si^{IV} atoms [43] not evidenced through XRD; as it happens, chemical shifts up to −60 and −70 ppm for cubic SiP_2O_7 have been previously reported [41,43]. Accordingly, the presence of these resonances in AP18.75P6.25, and only as traces in AP12.5MP6.25P6.25, could be related to phosphate linked to 6-fold coordinate Si structures, which have been already found with ^{29}Si NMR.

In summary, ^{29}Si and ^{27}Al suggest that fly ash is degraded with concomitant segregation of silica and octahedral Al-rich domains; but this phenomenon is partially hindered by the presence of melamine, probably due to its lower volatility with respect to ammonium cations. This is confirmed by the presence of peaks related to tetrahedral Al sites in AP12.5MP6.25P6.25. Accordingly, the phosphate reactivity towards the fly ash appears stronger in the binary AP18.75P6.25 sample. In fact, its ^{29}Si and ^{31}P spectra both indicate formation of silica and phosphosilicates with Si^{IV} and Si^{VI} units, and also a higher amount of pyrophosphates. The NMR results confirm the above mentioned role of melamine polyphosphate in the process, leading to the formation of different phases in a ternary composition such as AP12.5MP6.25P6.25.

4. Conclusions

The beneficial use of fly ash as a reactive component of flame retardant systems based on ammonium polyphosphate and melamine polyphosphate to improve the fire reaction of PLA has been shown. Synergistic effects on flame retardancy were achieved on the majority of fire parameters measured using PCFC and cone calorimeter. Except for the equimassic composition of ammonium polyphosphate and fly ash, all the compositions with fly ash exhibited lower pHRR values at PCFC than ammonium polyphosphate alone. The substitution of 25% of the amount of ammonium polyphosphate by fly ash allowed the pHRR and the MAHRE to be reduced with a significant increase of the weight of the residue, indicating the formation of new compounds in the condensed phase. A partial substitution of 33 wt% ammonium polyphosphate by melamine polyphosphate in PLA allowed the pHRR both for PCFC and cone calorimeter to be reduced significantly and to maintain the V-0 class. Finally, it appears that the selection of relevant fractions of the three above components in PLA could result in an improvement of the fire parameters in comparison with ammonium polyphosphate alone. Indeed, it has been shown that AP12.5MP6.25P6.25 and AP16.67MP8.33 behave similarly, despite a higher amount of fly ash in AP8.33MP4.17P12.5 does not appear to be particularly advantageous. Consequently, optimized amounts of fly ash are able to replace a significant fraction of phosphorous flame retardants in PLA without any loss in performance. This behavior may be attributed to new crystalline phases that appeared after the combustion of PLA containing the binary composition and are clearly identified as platelets organized in windroses. It is to be noted that the residue contains in addition a visible fraction of the fly ash that remained unreacted, as well as mullite and quartz that have been identified by X-Ray diffraction. From quantitative analysis of ^{27}Al NMR spectra, the existence of AlPO structures or Al-O-P compounds not detected by X-Ray diffraction can be inferred. The ^{29}Si spectrum shows that some 6-fold coordinated Si is present in the AP18.75P6.25 residue indicating that structures such as $Si_5O(PO_4)_6$ could also be present. ^{31}P NMR analyses suggests the formation of slightly ordered phosphate structures which could result from the reaction between phosphate groups with carbon from PLA or metallic ions from fly ash. Moreover, the ^{31}P and ^{29}Si spectra of AP18.75P6.25 residue suggests the formation of amorphous phosphosilicates close to SiP_2O_7 or $Si_5O(PO_4)_6$, with phosphate units linked to 6-fold coordinated Si, which were expected to be present in the form of crystalline components according to previous work.

Indeed, X-Ray diffraction suggests the formation of new phosphate compounds which correspond to different phases observed in the AP18.75P6.25 composition. The presence of Al-O-P compounds is also confirmed by ^{27}Al spectra. Nevertheless, for this composition, it can be stated from all NMR analyses that melamine seems to hinder the reactivity of fly ash towards polyphosphates.

CRediT authorship contribution statement

Marcos Batistella: Conceptualization, Methodology, Writing – original draft, Investigation. **Jean-Claude Roux:** Validation, Investigation, Writing – review & editing. **Gwenn le Saout:** Validation, Investigation, Writing – review & editing. **Emanuela Callone:** Investigation, Writing – original draft. **Sandra Diré:** Investigation, Writing – original draft. **Constantinos Xenopoulos:** Writing – review & editing, Supervision. **José-Marie Lopez-Cuesta:** Writing – original draft, Supervision, Project administration.

Declaration of Competing Interest

The authors declare that they have no known competing financial interests or personal relationships that could have appeared to influence the work reported in this paper.

Data availability

Data will be made available on request.

Supplementary materials

Supplementary material associated with this article can be found, in the online version, at doi:10.1016/j.polymdegradstab.2023.110314.

References

[1] R. Sonnier, A. Taguet, L. Ferry, J.M. Lopez-Cuesta, Towards Bio-based Flame Retardant Polymers, Springer International Publishing, Cham, 2018, https://doi.org/10.1007/978-3-319-67083-6.

[2] G. Camino, L. Costa, G. Martinasso, Intumescent fire-retardant systems, Polym. Degrad. Stab. 23 (1989) 359–376, https://doi.org/10.1016/0141-3910(89)90058-X.

[3] G. Camino, R. Delobel, A.F. Grand, C.A. Wilkie, Intumescence. Fire Retardant Polymeric Materials, 1st ed., CRC Press, New York, 2000.

[4] C. Réti, M. Casetta, S. Duquesne, S. Bourbigot, R. Delobel, Flammability properties of intumescent PLA including starch and lignin, Polym. Adv. Technol. 19 (2008) 628–635, https://doi.org/10.1002/pat.1130.

[5] X. Wang, Y. Hu, L. Song, S. Xuan, W. Xing, Z. Bai, H. Lu, Flame retardancy and thermal degradation of intumescent flame retardant poly(lactic acid)/starch biocomposites, Ind. Eng. Chem. Res. 50 (2011) 713–720, https://doi.org/10.1021/ie1017157.

[6] K. Wu, Y. Hu, L. Song, H. Lu, Z. Wang, Flame retardancy and thermal degradation of intumescent flame retardant starch-based biodegradable composites, Ind. Eng. Chem. Res. 48 (2009) 3150–3157, https://doi.org/10.1021/ie801230h.

[7] A. Cayla, F. Rault, S. Giraud, F. Salaün, V. Fierro, A. Celzard, PLA with intumescent system containing lignin and ammonium polyphosphate for flame retardant textile, Polymers 8 (2016) 331, https://doi.org/10.3390/polym8090331. Basel.

[8] R. Zhang, X. Xiao, Q. Tai, H. Huang, J. Yang, Y. Hu, The effect of different organic modified montmorillonites (OMMTs) on the thermal properties and flammability of PLA/MCAPP/lignin systems, J. Appl. Polym. Sci. 127 (2013) 4967–4973, https://doi.org/10.1002/app.38095.

[9] V. Carretier, J. Delcroix, M.F. Pucci, P. Rublon, J.M. Lopez-Cuesta, Influence of sepiolite and lignin as potential synergists on flame retardant systems in polylactide (PLA) and polyurethane elastomer (PUE), Materials 13 (2020), https://doi.org/10.3390/ma13112450. Basel.

[10] S. Yu, H. Xiang, J. Zhou, M. Zhu, Enhanced flame-retardant performance of poly (lactic acid) (PLA) composite by using intrinsically phosphorus-containing PLA, Prog. Nat. Sci. Mater. Int. 28 (2018) 590–597, https://doi.org/10.1016/j.pnsc.2018.09.002.

[11] X.Q. Liu, D.Y. Wang, X.L. Wang, L. Chen, Y.Z. Wang, Synthesis of organo-modified α-zirconium phosphate and its effect on the flame retardancy of IFR poly(lactic acid) systems, Polym. Degrad. Stab. 96 (2011) 771–777, https://doi.org/10.1016/j.polymdegradstab.2011.02.022.

[12] J.Z. Du, L. Jin, H.Y. Zeng, B. Feng, S. Xu, E.G. Zhou, X.K. Shi, L. Liu, X. Hu, Facile preparation of an efficient flame retardant and its application in ethylene vinyl acetate, Appl. Clay Sci. 168 (2019) 96–105, https://doi.org/10.1016/j.clay.2018.11.004.

[13] X.Q. Liu, D.Y. Wang, X.L. Wang, L. Chen, Y.Z. Wang, Synthesis of functionalized α-zirconium phosphate modified with intumescent flame retardant and its application in poly(lactic acid), Polym. Degrad. Stab. 98 (2013) 1731–1737, https://doi.org/10.1016/j.polymdegradstab.2013.06.001.

[14] Z. Li, D. Fernández Expósito, A. Jiménez González, D.Y. Wang, Natural halloysite nanotube based functionalized nanohybrid assembled via phosphorus-containing slow release method: a highly efficient way to impart flame retardancy to polylactide, Eur. Polym. J. 93 (2017) 458–470, https://doi.org/10.1016/j.eurpolymj.2017.06.021.

[15] R. Sonnier, L. Ferry, C. Longuet, F. Laoutid, B. Friederich, A. Laachachi, J.M. Lopez-Cuesta, Combining cone calorimeter and PCFC to determine the mode of action of flame-retardant additives, Polym. Adv. Technol. 22 (2011) 1091–1099, https://doi.org/10.1002/pat.1989.

[16] M. Lewin, Some comments on the modes of action of nanocomposites in the flame retardancy of polymers, Fire Mater. 27 (2003) 1–7, https://doi.org/10.1002/fam.813.

[17] H. Vahabi, R. Sonnier, B. Otazaghine, G.Le Saout, J.M. Lopez-Cuesta, Nanocomposites of polypropylene/polyamide 6 blends based on three different nanoclays: thermal stability and flame retardancy, Polimery Polym. 58 (2013) 350–360, https://doi.org/10.14314/polimery.2013.350.

[18] L. Dumazert, D. Rasselet, B. Pang, B. Gallard, S. Kennouche, J.M. Lopez-Cuesta, Thermal stability and fire reaction of poly(butylene succinate) nanocomposites using natural clays and FR additives, Polym. Adv. Technol. 29 (2018) 69–83, https://doi.org/10.1002/pat.4090.

[19] R.G. Puri, A.S. Khanna, Effect of cenospheres on the char formation and fire protective performance of water-based intumescent coatings on structural steel, Prog. Org. Coat. 92 (2016) 8–15, https://doi.org/10.1016/j.porgcoat.2015.11.016.

[20] I.I. Kabir, C.C. Sorrell, M.R. Mada, S.T. Cholake, S. Bandyopadhyay, General model for comparative tensile mechanical properties of composites fabricated from fly ash and virgin/recycled high-density polyethylene, Polym. Eng. Sci. 56 (2016) 1096–1108, https://doi.org/10.1002/pen.24342.

[21] E.V. Fomenko, N.N. Anshits, A.G. Anshits, The composition, structure, and helium permeability of glass-crystalline shells of cenospheres, Glass Phys. Chem. 45 (2019) 36–46, https://doi.org/10.1134/S1087659619010024.

[22] R.E. Lyon, R.N. Walters, Pyrolysis combustion flow calorimetry, J. Anal. Appl. Pyrolysis 71 (2004) 27–46, https://doi.org/10.1016/S0165-2370(03)00096-2.

[23] J.B. d'Espinose de Lacaillerie, C. Fretigny, D. Massiot, MAS NMR spectra of quadrupolar nuclei in disordered solids: the Czjzek model, J. Magn. Reson. 192 (2008) 244–251, https://doi.org/10.1016/j.jmr.2008.03.001.

[24] D. Massiot, F. Fayon, M. Capron, I. King, S.L. Calvé, B. Alonso, J.O. Durand, B. Bujoli, Z. Gan, G. Hoatson, Modelling one- and two-dimensional solid-state NMR spectra, Magn. Reson. Chem. 40 (2002) 70–76, https://doi.org/10.1002/mrc.984.

[25] Y. Xue, X. Zuo, L. Wang, Y. Zhou, Y. Pan, J. Li, Y. Yin, D. Li, R. Yang, M. H. Rafailovich, Y. Guo, Enhanced flame retardancy of poly(lactic acid) with ultra-low loading of ammonium polyphosphate, Compos. Part B Eng. 196 (2020), 108124, https://doi.org/10.1016/j.compositesb.2020.108124.

[26] A. Sut, E. Metzsch-Zilligen, M. Großhauser, R. Pfaendner, B. Schartel, Synergy between melamine cyanurate, melamine polyphosphate and aluminum diethylphosphinate in flame retarded thermoplastic polyurethane, Polym. Test. 74 (2019) 196–204, https://doi.org/10.1016/j.polymertesting.2019.01.001.

[27] L. Costa, G. Camino, M.P. Luda di Cortemiglia, Mechanism of thermal degradation of fire-retardant melamine salts. Fire Polym., 425th ed, American Chemical Society, Washington D.C., 1990, pp. 211–238.

[28] Y. Guo, C.C. Chang, M.A. Cuiffo, Y. Xue, X. Zuo, S. Pack, L. Zhang, S. He, E. Weil, M.H. Rafailovich, Engineering flame retardant biodegradable polymer nanocomposites and their application in 3D printing, Polym. Degrad. Stab. 137 (2017) 205–215, https://doi.org/10.1016/j.polymdegradstab.2017.01.019.

[29] G. Fontaine, S. Bourbigot, Intumescent polylactide: a nonflammable material, J. Appl. Polym. Sci. 113 (2009) 3860–3865, https://doi.org/10.1002/app.30379.

[30] M. Lewin, E.M. Pearce, K. Levon, A. Mey-Marom, M. Zammarano, C.A. Wilkie, B. N. Jang, Nanocomposites at elevated temperatures: migration and structural changes, Polym. Adv. Technol. 17 (2006) 226–234, https://doi.org/10.1002/pat.684.

[31] M. Lewin, E... Weil, A.R. Horrocks, D. Price, Mechanisms and modes of action in flame retardancy of polymers. Fire Retardant Materials, Woodhead Publishing, Cambridge, 2001, p. 39.

[32] H.D. Morris, S. Bank, P.D. Ellis, Aluminum-27 NMR spectroscopy of iron-bearing montmorillonite clays, J. Phys. Chem. 94 (1990) 3121–3129, https://doi.org/10.1021/j100370a069.

[33] E. Callone, R. Ceccato, F. Deflorian, M. Fedel, S. Dirè, Filler-matrix interaction in sodium montmorillonite-organosilica nanocomposite coatings for corrosion protection, Appl. Clay Sci. 150 (2017) 81–88, https://doi.org/10.1016/j.clay.2017.09.016.

[34] X. Pardal, F. Brunet, T. Charpentier, I. Pochard, A. Nonat, 27 Al and 29 Si Solid-State NMR characterization of calcium-aluminosilicate-hydrate, Inorg. Chem. 51 (2012) 1827–1836, https://doi.org/10.1021/ic202124x.

[35] D.R. Neuville, L. Cormier, D. Massiot, Al coordination and speciation in calcium aluminosilicate glasses: effects of composition determined by 27Al MQ-MAS NMR and Raman spectroscopy, Chem. Geol. 229 (2006) 173–185, https://doi.org/10.1016/j.chemgeo.2006.01.019.

[36] M.A. Harmer, A.J. Vega, Nuclear magnetic resonance study of a high-surface-area aluminum phosphate glass and its thermally reversible sol-gel precursor, Solid State Nucl. Magn. Reson. 5 (1995) 35–49, https://doi.org/10.1016/0926-2040(95)00036-P.

[37] B. Walkley, J.L. Provis, Solid-state nuclear magnetic resonance spectroscopy of cements, Mater. Today Adv. 1 (2019), 100007, https://doi.org/10.1016/j.mtadv.2019.100007.

[38] P. Straka, Characterization of aluminum(III) complexes in coal organic matter, Am. J. Anal. Chem. 07 (2016) 378–394, https://doi.org/10.4236/ajac.2016.74036.

[39] M. Haouas, F. Taulelle, C. Martineau, Recent advances in application of 27Al NMR spectroscopy to materials science, Prog. Nucl. Magn. Reson. Spectrosc. 94–95 (2016) 11–36, https://doi.org/10.1016/j.pnmrs.2016.01.003.

[40] J.F. Ortiz-Mosquera, A.M. Nieto-Muñoz, H. Bradtmüller, H. Eckert, A.C. M. Rodrigues, Isothermal evolution of phase composition, structural parameters, and ionic conductivity in Na1+Al Ge2-(PO4)3 glass-ceramics, J. Non Cryst. Solids 533 (2020), 119725, https://doi.org/10.1016/j.jnoncrysol.2019.119725.

[41] C. Lejeune, C. Coelho, L. Bonhomme-Coury, T. Azaïs, J. Maquet, C. Bonhomme, Studies of silicophosphate derivatives by 31P→29Si CP MAS NMR, Solid State Nucl. Magn. Reson. 27 (2005) 242–246, https://doi.org/10.1016/j.ssnmr.2005.02.001.

[42] L. Martel, A. Kovács, K. Popa, D. Bregiroux, T. Charpentier, 31P MAS NMR and DFT study of crystalline phosphate matrices, Solid State Nucl. Magn. Reson. 105 (2020), 101638, https://doi.org/10.1016/j.ssnmr.2019.101638.

[43] M. Coquelle, S. Duquesne, M. Casetta, J. Sun, X. Gu, S. Zhang, S. Bourbigot, Flame Retardancy of PA6 using a guanidine sulfamate/melamine polyphosphate mixture, Polymers 7 (2015) 316–332, https://doi.org/10.3390/polym7020316. Basel.

[44] A.D. Naik, G. Fontaine, F. Samyn, X. Delva, J. Louisy, S. Bellayer, Y. Bourgeois, S. Bourbigot, Outlining the mechanism of flame retardancy in polyamide 66 blended with melamine-poly(zinc phosphate), Fire Saf. J. 70 (2014) 46–60, https://doi.org/10.1016/j.firesaf.2014.08.019.

[45] Y. Yu, H. Guo, M. Pujari-Palmer, B. Stevensson, J. Grins, H. Engqvist, M. Edén, Advanced solid-state 1H/31P NMR characterization of pyrophosphate-doped calcium phosphate cements for biomedical applications: the structural role of pyrophosphate, Ceram. Int. 45 (2019) 20642–20655, https://doi.org/10.1016/j.ceramint.2019.07.047.

[46] C. Coelho, T. Azais, L. Bonhomme-Coury, J. Maquet, D. Massiot, C. Bonhomme, Application of the MAS-J-HMQC experiment to a new pair of nuclei {29Si,31P}: si5O(PO4)6 and SiP2O7 polymorphs, J. Magn. Reson. 179 (2006) 114–119, https://doi.org/10.1016/j.jmr.2005.11.015.